J. Fluid Mech. (1998), *vol.* 370, *pp.* 249–270. Printed in the United Kingdom

Bacterial bioconvection: weakly nonlinear theory for pattern selection

By A. M. METCALFE[1] AND T. J. PEDLEY[2]

[1] Department of Applied Mathematical Studies, University of Leeds, Leeds, LS2 9JT, UK

[2] Department of Applied Mathematics and Theoretical Physics, University of Cambridge, Silver Street, Cambridge CB3 9EW, UK

(Received 31 July 1997 and in revised form 7 January 1998)

Complex bioconvection patterns are observed when a suspension of the oxytactic bacterium *Bacillus subtilis* is placed in a chamber with its upper surface open to the atmosphere. The patterns form because the bacteria are denser than water and swim upwards (up an oxygen gradient) on average. This results in an unstable density distribution and an overturning instability. The pattern formation is dependent on depth and experiments in a tilted chamber have shown that as the depth increases the first patterns formed are hexagons in which the fluid flows down in the centre.

The linear stability of this system was analysed by Hillesdon & Pedley (1996) who found that the system is unstable if the Rayleigh number Γ exceeds a critical value, which depends on the wavenumber k of the disturbance as well as on the values of other parameters. Hillesdon & Pedley found that the critical wavenumber k_c could be either zero or non-zero, depending on the parameter values.

In this paper we carry out a weakly nonlinear analysis to determine the relative stability of hexagon and roll patterns formed at the onset of bioconvection. The analysis is different in the two cases $k_c \neq 0$ and $k_c = 0$. For the $k_c \neq 0$ case (which appears to be more relevant experimentally) the model does predict down hexagons, but only for a certain range of parameter values. Hence the analysis allows us to refine previous parameter estimates. For the $k_c = 0$ case we carry out a two-dimensional analysis and derive an equation describing the evolution of the horizontal planform function.

1. Introduction

The spontaneous formation of bioconvection patterns has been observed in suspensions of swimming microorganisms such as the alga *Chlamydomonas nivalis* and the bacterium *Bacillus subtilis* (Wager 1911; Platt 1961; Pedley & Kessler 1992; Kessler *et al.* 1994, 1995). Much of the previous work on bioconvection has concentrated on algae; in this paper we consider bioconvection in a suspension of swimming bacteria in which the upswimming is due to aerotaxis (swimming up oxygen gradients).

B. subtilis is a harmless soil bacterium which swims by rotating its flagellar bundle. It consumes oxygen and on average swims up oxygen gradients. In common with other chemotactic bacteria such as *Escherichia coli*, *B. subtilis* does not swim in a uniform straight line up the chemoattractant gradient but rather the cell swimming direction is random, with merely a mean 'drift' in the preferred direction (Berg & Brown 1972; Alt 1994; Kessler *et al.* 1995). In the model to be described this

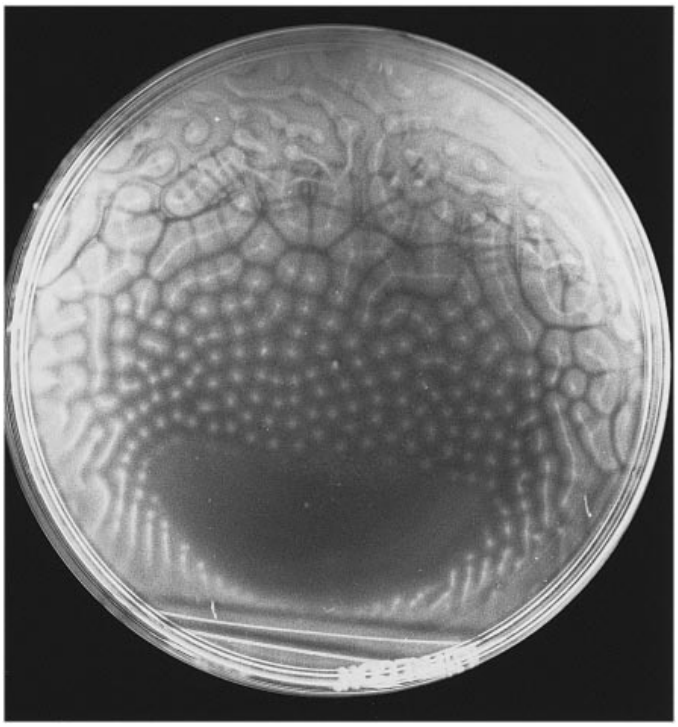

FIGURE 1. Bioconvection pattern in a suspension of *B. subtilis* in a tilted chamber. There are no patterns in the shallow region at the bottom of the photograph. As the depth increases a pattern of hexagons is seen which gives way to more complex patterns as the depth increases further. The walls and meniscus affect the patterns at the edges of the petri dish. Light areas represent regions of high bacterial concentration in which the fluid is descending. Photograph courtesy of J. O. Kessler.

swimming is represented as an isotropic cell diffusion with a superimposed average swimming velocity proportional to the concentration gradient of the chemoattractant (Keller & Segel 1971*a*, *b*).

The experiment of Kessler *et al.* (1994) consists of an initially well-stirred suspension of *B. subtilis* with uniform concentrations of both oxygen and bacteria. The bacteria consume oxygen throughout the suspension but oxygen is only replenished at the free surface, causing an oxygen gradient to be set up. The bacteria then swim up this oxygen gradient leading to an unstable density distribution which results in an overturning instability and the formation of patterns. The instability is analogous to Rayleigh–Bénard convection, hence the term bioconvection.

Figure 1 shows the bioconvection patterns set up in a tilted petri dish in which the depth of the suspension varies. In the very shallow regions (near the bottom of the photograph) no patterns are formed. As the depth increases above a critical value a band of hexagons is seen which gives way to more complicated roll-type patterns as the depth increases further. The weakly nonlinear analysis described in this paper can be used to predict the patterns when the suspension is just deep enough for patterns to be formed. In figure 1 the light areas represent regions with a high concentration of bacteria in which the fluid is falling. Hence the hexagons formed when the depth is slightly supercritical are ‘down’ hexagons in which fluid flows down in the centre and up at the edges.

Previous work on the problem of bacterial bioconvection has involved setting up the model equations, tracing the evolution towards a steady-state (Hillesdon, Pedley & Kessler 1995) and investigating the linear stability of such steady-state solutions (Hillesdon & Pedley 1996). Here we summarize some of the previous results (§§ 2 and 3) before describing a weakly nonlinear analysis of the problem for suspensions that are not so deep that the oxygen concentration falls effectively to zero near the bottom. There are two distinct cases to be considered, one in which the critical wavenumber from linear theory is non-zero (§§ 4 and 5) and one in which it is zero (§ 6).

In the non-zero critical wavenumber case the weakly nonlinear analysis allows us to draw a bifurcation diagram describing the behaviour of the system. For certain values of the parameters the model predicts the formation of down hexagons with a wavelength close to that observed in experiment. In the zero critical wavenumber case we consider two-dimensional patterns and use a long-wavelength approximation to derive an equation describing the evolution of the horizontal planform.

2. The model

The problem is described by an equation for cell concentration (N) and an equation for oxygen concentration (C), together with the Navier–Stokes equations and the continuity equation. The equation for cell conservation is

$$\frac{\partial N}{\partial T} = -\nabla \cdot (N\boldsymbol{U} + N\boldsymbol{V} - \boldsymbol{D}_N \cdot \nabla N), \tag{2.1}$$

in which the cell flux vector contains a term for advection of cells with the bulk fluid velocity $\boldsymbol{U}$ and two terms describing cell swimming. The diffusive term ($\boldsymbol{D}_N \cdot \nabla N$) describes the random aspects of cell swimming and $\boldsymbol{V}$ is the superimposed average swimming velocity. The equation for oxygen conservation is

$$\frac{\partial C}{\partial T} = -\nabla \cdot (C\boldsymbol{U} - D_C \nabla C) - KN, \tag{2.2}$$

where the oxygen flux vector contains terms for advection and diffusion of oxygen (where D_C is the oxygen diffusivity) and K is the rate of oxygen consumption by the bacteria.

If the suspension is sufficiently dilute for hydrodynamic cell–cell interactions to be negligible, the equations for the fluid velocity are the continuity equation and the Navier–Stokes equations under the Boussinesq approximation:

$$\nabla \cdot \boldsymbol{U} = 0, \tag{2.3}$$

$$\rho_w \left(\frac{\partial \boldsymbol{U}}{\partial T} + (\boldsymbol{U} \cdot \nabla)\boldsymbol{U} \right) = -\nabla P_e + v(\rho_c - \rho_w) N \boldsymbol{g} + \mu \Delta \boldsymbol{U}. \tag{2.4}$$

Here ρ_w and ρ_c are the densities of water and cells respectively, μ is the viscosity of the suspension, v is the volume of one cell, $P_e(\boldsymbol{X}, T)$ is the excess pressure above hydrostatic and $\boldsymbol{g}$ is the acceleration due to gravity.

The timescale over which patterns form, of the order of minutes, is very much smaller than the timescale for bacterial reproduction, which is several hours; therefore there is no term for bacterial reproduction or death in (2.1). We have also neglected the contribution to $\boldsymbol{D}_N$ from Brownian motion and to $\boldsymbol{V}$ from cell sedimentation since both of these are small compared to the corresponding contributions from cell swimming (Hillesdon *et al.* 1995). For simplicity we also ignore the effect of gyrotaxis (the orientation of the cells by viscous forces in a shear flow) although this has been

found to be important in bioconvection of algae such as *C. nivalis* (Kessler 1985; Hill, Pedley & Kessler 1989; Pedley & Kessler 1990) and is probably important in the bacterial case also.

The behaviour of the bacteria can be thought of as requiring a minimum concentration of oxygen, C_{min}, in order to be active. This is taken into account by non-dimensionalising the oxygen concentration as $\theta = (C - C_{min})/(C_0 - C_{min})$, where C_0 is the initial and free-surface oxygen concentration. The cell diffusion is modelled as an isotropic tensor $\boldsymbol{D}_N = D_{N0}H(\theta)\boldsymbol{I}$, the directional cell swimming as proportional to the gradient of θ, $\boldsymbol{V} = aV_sH(\theta)\nabla\theta$ and the oxygen consumption as $K = K_0H(\theta)$. D_{N0} and aV_s are taken to be given constants; a has dimensions of length so that V_s has dimensions of velocity. The cut-off is modelled using the Heaviside step function $H(\theta)$ since this gives us an analytic solution for the steady state in a shallow chamber. Hillesdon *et al.* (1995) also considered modelling the cut-off in a slightly more realistic manner using a function which saturates exponentially. In that case the steady-state solution was found numerically. No qualitative difference was found for the results in a shallow chamber, hence for simplicity we use the step function form of the cut-off.

The other variables are non-dimensionalized as

$$n = \frac{N}{N_0}, \qquad z = \frac{Z}{h}, \qquad t = \frac{D_{N0}}{h^2}\,T, \qquad \boldsymbol{u} = \frac{h}{D_{N0}}\,\boldsymbol{U}, \qquad p_e = \frac{h^2}{\mu D_{N0}}\,P_e,$$

where h is the depth of the chamber and N_0 is the initial cell concentration. The vertical coordinate z is measured downwards so that $z = 1$ is the bottom of the chamber and $z = 0$ is the free surface at the top. Unlike the experiment of figure 1, the depth of the chamber in the model is uniform and we assume that the free surface is planar. The non-dimensionalized equations are

$$\frac{\partial n}{\partial t} = \nabla\cdot[H(\theta)\nabla n - \boldsymbol{u}n - H(\theta)\gamma n\nabla\theta], \tag{2.5}$$

$$\frac{\partial \theta}{\partial t} = \nabla\cdot(\delta\nabla\theta - \boldsymbol{u}\theta) - H(\theta)\delta\beta n, \tag{2.6}$$

$$Sc^{-1}\left[\frac{\partial \boldsymbol{u}}{\partial t} + (\boldsymbol{u}\cdot\nabla)\boldsymbol{u}\right] = -\nabla p_e + \Gamma n\hat{\boldsymbol{z}} + \Delta\boldsymbol{u}, \tag{2.7}$$

$$\nabla\cdot\boldsymbol{u} = 0, \tag{2.8}$$

where the dimensionless parameters are

$$\beta = \frac{K_0N_0h^2}{D_C(C_0 - C_{min})}, \qquad \gamma = \frac{aV_s}{D_{N0}}, \qquad \delta = \frac{D_C}{D_{N0}},$$

$$\Gamma = \frac{v\alpha N_0gh^3}{vD_{N0}}, \qquad Sc = v/D_{N0}, \qquad v = \mu/\rho_w,$$

where $\alpha = (\rho_c - \rho_w)/\rho_w$. The parameter β, which represents the strength of oxygen consumption relative to its diffusion, can also be regarded as a depth parameter; γ is a measure of the relative strengths of directional and random swimming and δ is the ratio of oxygen diffusivity to cell diffusivity. Γ is analogous to the Rayleigh number in thermal convection and Sc is a Schmidt number.

A no-slip condition is imposed at the bottom of the chamber and a stress-free condition at the free surface. The other boundary conditions are zero vertical component of fluid velocity at the upper and lower boundaries, zero cell flux at all boundaries,

zero oxygen flux at the bottom and $C = C_0$ at the free surface. These boundary conditions are thus:
at $z = 0$

$$\boldsymbol{u}\cdot\hat{\boldsymbol{z}} = 0, \qquad \frac{\partial^2}{\partial z^2}(\boldsymbol{u}\cdot\hat{\boldsymbol{z}}) = 0, \qquad \theta = 1, \qquad H(\theta)\frac{\partial n}{\partial z} - \gamma n H(\theta)\frac{\partial \theta}{\partial z} = 0;$$

at $z = 1$

$$\boldsymbol{u}\cdot\hat{\boldsymbol{z}} = 0, \qquad \boldsymbol{u}\times\hat{\boldsymbol{z}} = 0, \qquad \frac{\partial \theta}{\partial z} = 0, \qquad \frac{\partial n}{\partial z} = 0.$$

Integrating equation (2.5) over a volume, V, gives

$$\int_V n \, \mathrm{d}\boldsymbol{x} = \text{const} = 1 \,, \tag{2.9}$$

which represents conservation of cells. The integral is from 0 to 1 with respect to z and the horizontal domain is either such that n, θ and $\boldsymbol{u}$ are periodic over it, or is the horizontal extent of the chamber.

3. Steady-state solution and linear stability theory

In the steady state diffusion of cells (random cell swimming) balances chemotaxis (mean swimming up the oxygen gradient), while oxygen diffusion is balanced by oxygen consumption. The steady-state distributions of bacteria (n_0) and oxygen (θ_0) depend only on z. There are two distinct cases. In a 'shallow' chamber (see figure 2) the oxygen concentration is greater than C_{min}, i.e. $\theta > 0$, throughout the suspension, which means that all the cells are actively swimming and consuming oxygen. In the 'deep' chamber case the oxygen concentration below a certain depth falls to C_{min} (i.e. $\theta = 0$) and the bacteria in this lower, oxygen-depleted region become inactive and cease to swim or to consume oxygen (figure 3). For a deep chamber there is no closed-form solution to the steady-state problem but for the shallow chamber such a solution does exist:

$$\theta_0 = 1 - \frac{2}{\gamma}\ln\left\{\frac{\cos\left(\frac{1}{2}A(1-z)\right)}{\cos\left(\frac{1}{2}A\right)}\right\}, \tag{3.1}$$

$$n_0 = \frac{A^2}{2\beta\gamma}\sec^2\left(\tfrac{1}{2}A(1-z)\right), \tag{3.2}$$

where

$$\tan\left(\frac{A}{2}\right) = \frac{\beta\gamma}{A}.$$

θ_0 is positive for all $z < 1$, and the chamber is, in this sense, shallow if

$$\beta \leqslant \frac{2}{\gamma}\phi \arctan\phi, \tag{3.3}$$

where $\phi = (\mathrm{e}^{\gamma} - 1)^{1/2}$ (see Hillesdon *et al.* 1995). In this paper we consider only the shallow case.

The linear stability of the steady state depends on the Rayleigh number Γ. If Γ is less than some critical value Γ_n the steady state is stable whereas if Γ is greater than Γ_n the steady state is unstable. Γ_n depends on the wavenumber k of the disturbance. The wavenumber k_c for which Γ_n has its minimum value Γ_c is the most unstable wavenumber and as Γ increases the first bifurcation will be to disturbances

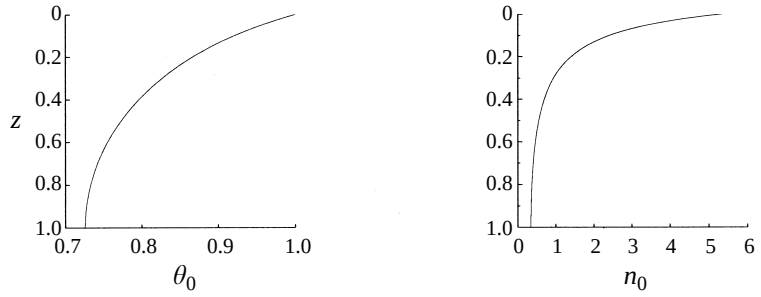

FIGURE 2. The steady-state oxygen, θ_0, and cell, n_0, distributions for a shallow chamber ($\beta = 1$, $\gamma = 10$, $\delta = 1$).

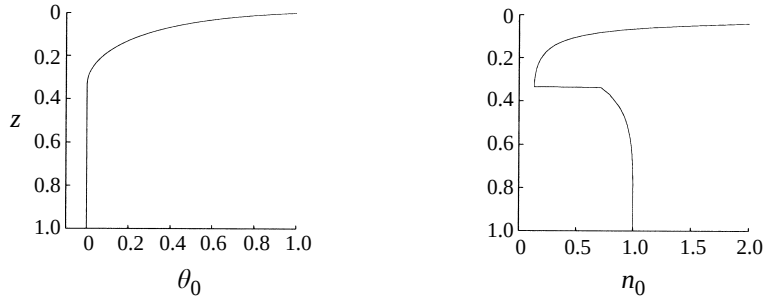

FIGURE 3. The steady-state oxygen, θ_0, and cell, n_0, distributions for a deep chamber ($\beta = 60$, $\gamma = 5$, $\delta = 1$).

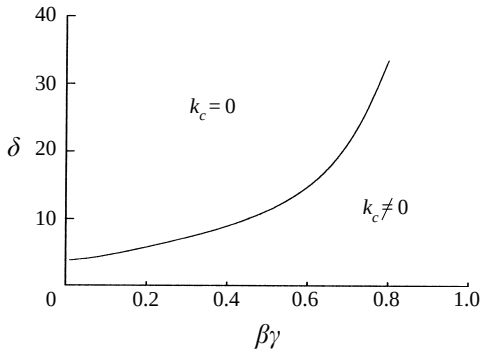

FIGURE 4. Regions of parameter space where the critical wavenumber k_c is zero and non-zero.

of wavelength $2\pi/k_c$. Hillesdon & Pedley (1996) computed the values of k_c and Γ_c, which depend on δ and the combination $\beta\gamma$. In particular k_c can be either zero or non-zero: the regions of parameter space in which k_c is zero or non-zero are shown in figure 4.

The linear analysis predicts the wavelength of the patterns formed, but to predict the type of pattern requires a weakly nonlinear analysis. The two cases $k_c = 0$ and $k_c \neq 0$ must be treated separately. The calculation for $k_c \neq 0$ will be presented first, followed by the calculation for $k_c = 0$.

4. Weakly nonlinear analysis: $k_c \neq 0$

The aim of the weakly nonlinear analysis is to predict the patterns formed when the Rayleigh number Γ is near critical. Three types of pattern are commonly seen in convection problems: rolls, squares and hexagons. There are two types of hexagon: those in which flow is up in the centre and down at the edges (up hexagons) and those in which flow is down in the centre and up at the edges (down hexagons). The calculation can be simplified by considering either patterns which fit on a hexagonal lattice (rolls and hexagons) or those which fit on a square lattice (rolls and squares). It is not possible to compare the relative stability of hexagons and squares since they do not fit on the same lattice. Since hexagons are observed experimentally we restict our calculation to the hexagonal lattice. The method is similar to that used by Matthews (1988), among others.

The symmetries of the system restrict the possible solutions. In an up–down asymmetric problem such as this both roll and hexagon bifurcations from the steady state are unstable near the bifurcation point (Buzano & Golubitsky 1983; Golubitsky, Swift & Knobloch 1984). One or more of these patterns may be stabilized at finite amplitude; commonly hexagons are stabilized at a lower value of the Rayleigh number than rolls (see figure 5 below, which is similar to the diagrams of Buzano & Golubitsky 1983; Golubitsky *et al.* 1984). A wider class of patterns may be stable near the bifurcation point in up–down symmetric systems.

The variables are expanded in terms of a small parameter ϵ which measures the departure of the Rayleigh number Γ from its critical value Γ_c. At each order in ϵ a solvability condition is derived which gives rise to an equation describing the evolution of the amplitude of the pattern.

The variables are expanded as

$$\left.\begin{array}{l} \Gamma = \Gamma_c + \epsilon\Gamma_1, \quad \boldsymbol{u} = \epsilon\boldsymbol{u}_1 + \epsilon^2\boldsymbol{u}_2 + \ldots, \quad n = n_0 + \epsilon n_1 + \epsilon^2 n_2 + \ldots, \\ \theta = \theta_0 + \epsilon\theta_1 + \epsilon^2\theta_2 + \ldots, \quad p = p_e + \epsilon p_1 + \epsilon^2 p_2 + \ldots. \end{array}\right\} \tag{4.1}$$

The evolution of the system over a slow timescale τ is studied, where $\tau = \epsilon t$. The expanded variables (4.1) are substituted into equations (2.5)–(2.8) and terms of the same order in ϵ equated.

At $O(1)$ we obtain the equations for the steady state $n_0(z)$ and $\theta_0(z)$.

At $O(\epsilon)$ the problem is the linear one solved by Hillesdon & Pedley (1996), in which the variables n_1, θ_1 and the vertical velocity w_1 are expressed as

$$n_1 = N(z)\, f(x,y), \quad \theta_1 = C(z)\, f(x,y), \quad w_1 = W(z)\, f(x,y).$$

On a hexagonal lattice the horizontal planform function $f(x,y)$ is

$$f(x,y) = \mathrm{Re}\left(A_1(\tau)\mathrm{e}^{\mathrm{i}ky} + A_2(\tau)\mathrm{e}^{-\frac{1}{2}\sqrt{3}\mathrm{i}kx - \frac{1}{2}\mathrm{i}ky} + A_3(\tau)\mathrm{e}^{\frac{1}{2}\sqrt{3}\mathrm{i}kx - \frac{1}{2}\mathrm{i}ky}\right); \tag{4.2}$$

for rolls we can take $A_1 = A$ and $A_2 = A_3 = 0$ and for hexagons $A_1 = A_2 = A_3 = A$.

The $O(\epsilon^2)$ problem then gives rise to the solvability condition:

$$\int \boldsymbol{v}\cdot\boldsymbol{R}\, \mathrm{d}\boldsymbol{x} + \iint \left(v_2\gamma n_1 \frac{\partial\theta_1}{\partial z}\right)\bigg|_{z=0} \mathrm{d}x\, \mathrm{d}y = 0, \tag{4.3}$$

where $\boldsymbol{v} = (v_1, v_2, v_3)$ represents the first-order adjoint variables to (w_1, n_1, θ_1) and $\boldsymbol{R}$ is the right-hand side of the $O(\epsilon^2)$ equations and consists of known first-order functions.

Equation (4.3) is really three solvability conditions, obtained by setting $\boldsymbol{v} = \boldsymbol{V}(z)\ \bar{A}_1\mathrm{e}^{-\mathrm{i}ky}$, $\boldsymbol{v} = \boldsymbol{V}(z)\ \bar{A}_2\mathrm{e}^{\frac{1}{2}\sqrt{3}\mathrm{i}kx + \frac{1}{2}\mathrm{i}ky}$ and $\boldsymbol{v} = \boldsymbol{V}(z)\ \bar{A}_3\mathrm{e}^{-\frac{1}{2}\sqrt{3}\mathrm{i}kx + \frac{1}{2}\mathrm{i}ky}$ in (4.3), where $\boldsymbol{V}(z) = (V_1, V_2, V_3)$ and an overbar represents the complex conjugate. Substituting in

the known first-order functions and integrating from 0 to $4\pi/\sqrt{3}k$ with respect to x and from 0 to $4\pi/k$ with respect to y gives:

$$\chi_1 \frac{\mathrm{d}A_1}{\mathrm{d}\tau} + \Gamma_1 \chi_3 A_1 + \chi_2 \bar{A}_2 \bar{A}_3 = 0 \tag{4.4}$$

and two more equations obtained by cyclic permutation of the A_i. The χ_i are integrals of the known first-order functions which are given in the Appendix.

For steady rolls where $A_1 = A$, $A_2 = A_3 = 0$ and $\mathrm{d}A/\mathrm{d}\tau = 0$, the solvability conditions imply that $\Gamma_1 = 0$. This indicates that for rolls we should have defined ϵ by $\Gamma - \Gamma_c = \epsilon^2 \Gamma_2$ and scaled time as $\tau = \epsilon^2 t$.

For steady hexagons where $A_1 = A_2 = A_3 = A$ and $\mathrm{d}A/\mathrm{d}\tau = 0$ the solvability conditions imply that

$$\Gamma_1 = -\frac{\chi_2}{\chi_3} A. \tag{4.5}$$

A stability analysis of (4.4) shows that both branches of this bifurcation are unstable. However, one of the branches may become stable at higher order. To capture this behaviour we rescale Γ and τ and include third-order (cubic) terms as well as the quadratic second-order terms in the amplitude equations. This mixing of second- and third-order terms is formally valid as long as the coefficient χ_2 can be taken to be $O(\epsilon)$ (Hoyle, McFadden & Davis 1996). Equation (4.5) then implies that $\Gamma - \Gamma_c$ is $O(\epsilon^2)$.

We redefine ϵ by

$$\Gamma = \Gamma_c + \epsilon^2 \Gamma_2$$

and let

$$\tau = \epsilon^2 t\,.$$

We again obtain the steady-state equations at $O(1)$ and the linear equations at $O(\epsilon)$. We wish to include both $O(\epsilon^2)$ and $O(\epsilon^3)$ terms in the amplitude equations, therefore we take the $O(\epsilon^2)$ and $O(\epsilon^3)$ terms together and derive the solvability condition

$$\begin{aligned} &\epsilon^3 \int \boldsymbol{v} \cdot \boldsymbol{Q}\, \mathrm{d}\boldsymbol{x} + \epsilon^2 \int \boldsymbol{v} \cdot \tilde{\boldsymbol{R}}\, \mathrm{d}\boldsymbol{x} \\ &\quad = -\epsilon^3 \iint \left(v_2 \gamma n_1 \frac{\partial \theta_2}{\partial z} + v_2 \gamma n_2 \frac{\partial \theta_1}{\partial z} \right)\Bigg|_{z=0} \mathrm{d}x\, \mathrm{d}y - \epsilon^2 \iint \left(v_2 \gamma n_1 \frac{\partial \theta_1}{\partial z} \right)\Bigg|_{z=0} \mathrm{d}x\, \mathrm{d}y, \end{aligned} \tag{4.6}$$

where $\tilde{\boldsymbol{R}}$ and $\boldsymbol{Q}$ contain known first- and second-order functions.

We then substitute the known first- and second-order functions into (4.6) to obtain three amplitude equations:

$$\epsilon^3 \chi_1 \frac{\mathrm{d}A_1}{\mathrm{d}\tau} + \epsilon^3 \Gamma_2 \chi_3 A_1 + \epsilon^3 \chi_6 A_1^2 \bar{A}_1 + \epsilon^3 \chi_5 A_1 \left(A_2 \bar{A}_2 + A_3 \bar{A}_3 \right) + \epsilon^2 \chi_2 \bar{A}_2 \bar{A}_3 = 0 \tag{4.7}$$

and the two further equations which are formed by cyclic permutations of the A_i. In this equation χ_1, χ_2 and χ_3 are the same as before and χ_5 and χ_6 are also given in the Appendix. If we assume that $\chi_1 \neq 0$, which is true for all cases studied numerically, we can write $\tilde{\chi}_2 = \chi_2/\chi_1$, $\tilde{\chi}_3 = \chi_3/\chi_1$ etc. and the amplitude equations become

$$\frac{\mathrm{d}A_1}{\mathrm{d}\tau} + \Gamma_2 \tilde{\chi}_3 A_1 + \tilde{\chi}_6 A_1^2 \bar{A}_1 + \tilde{\chi}_5 A_1 \left(A_2 \bar{A}_2 + A_3 \bar{A}_3 \right) + \frac{\tilde{\chi}_2}{\epsilon} \bar{A}_2 \bar{A}_3 = 0. \tag{4.8}$$

For regular, time-independent hexagons with $A_1 = A_2 = A_3 = A$ this amplitude

equation gives

$$\epsilon^2 \Gamma_2 = -\frac{(2\tilde{\chi}_5 + \tilde{\chi}_6)}{\tilde{\chi}_3}\epsilon^2 A^2 - \frac{\tilde{\chi}_2}{\tilde{\chi}_3}\epsilon A\,,$$

which means that

$$\Gamma = \Gamma_c - \epsilon\left(\frac{\tilde{\chi}_2}{\tilde{\chi}_3}\right)A - \epsilon^2\left(\frac{2\tilde{\chi}_5 + \tilde{\chi}_6}{\tilde{\chi}_3}\right)A^2. \tag{4.9}$$

Equation (4.9) indicates that we are justified in mixing the second- and third-order terms only if the ratio $\chi_2/(2\chi_5 + \chi_6)$ is $O(\epsilon)$. This ratio is certainly small ($\leqslant 0.1$) for almost all the parameter values we have investigated (see table 1 in § 5), but there is no proof that it must be small; in this sense an analysis such as this remains to some extent an *ad hoc* model, not a fully rational theory. A stability analysis of (4.8) shows that hexagons are stable only when

$$\tilde{\chi}_2 A < 0, \quad -\frac{\tilde{\chi}_2}{\epsilon}A - 2\tilde{\chi}_6 A^2 - 4\tilde{\chi}_5 A^2 < 0, \quad 2\frac{\tilde{\chi}_2}{\epsilon}A - 2\tilde{\chi}_6 A^2 + 2\tilde{\chi}_5 A^2 < 0.$$

For steady rolls ($A_1 = A$, $A_2 = A_3 = 0$) the solvability condition implies

$$\Gamma_2 = -\frac{\tilde{\chi}_6}{\tilde{\chi}_3}A^2. \tag{4.10}$$

This is a pitchfork bifurcation which has stable branches if

$$\tilde{\chi}_6 > 0, \quad A^2(\tilde{\chi}_6 - \tilde{\chi}_5) + \frac{\tilde{\chi}_2}{\epsilon}A < 0, \quad A^2(\tilde{\chi}_6 - \tilde{\chi}_5) - \frac{\tilde{\chi}_2}{\epsilon}A < 0.$$

The roll and hexagon branches are linked by a branch of mixed mode solutions of the form $A_1 = A$, $A_2 = A_3 = B$. These mixed mode solutions are rolls when $B = 0$ and regular hexagons when $B = A$. A stability analysis indicates that they are always unstable.

The shape and stability properties of the bifurcation diagram depend on the values of $\tilde{\chi}_2$, $\tilde{\chi}_3$, $\tilde{\chi}_5$ and $\tilde{\chi}_6$. We describe here only the cases relevant to our numerical results. The bifurcation diagrams are sketched in figure 5: they show the change in the amplitude of the disturbance, A, as the Rayleigh number Γ is increased. For simplicity we have drawn the diagrams as though the roll and hexagon branches lie in the same plane, but in reality they lie in different planes and do not intersect. Points where the different solution branches do intersect are marked with dots in the diagrams. The roll, hexagon and mixed mode branches are labelled R, H and M respectively. The hexagon branches with A positive represent up hexagons and those with A negative represent down hexagons. There is no difference between rolls with A positive or negative. In the diagrams we have drawn the roll branches with A positive except in cases where the diagram is clearer if A is taken as negative for rolls.

If $\tilde{\chi}_2 < 0$, $\tilde{\chi}_3 < 0$, $\tilde{\chi}_6 > \tilde{\chi}_5 > 0$ the bifurcation diagram will resemble figure 5(*a*). The stable branch of hexagons has A positive so we expect the first observed pattern to consist of up hexagons of finite amplitude, in which the flow is up in the centre and down at the edges. The rolls are supercritical and always unstable.

If $\tilde{\chi}_2 < 0$, $\tilde{\chi}_3 < 0$, $\tilde{\chi}_5 > \tilde{\chi}_6 > 0$ the bifurcation diagram will resemble figure 5(*b*). The first transition will again be to up hexagons but as Γ increases these hexagons lose stability and rolls become stable. Note the fact that there would, in practice, be hysteresis in the roll/hexagon transition (near the unstable branch M), as well as in the no-flow/hexagon transition (at the transcritical bifurcation Γ_c).

If $\tilde{\chi}_2 > 0$, $\tilde{\chi}_3 < 0$, $\tilde{\chi}_5 > \tilde{\chi}_6 > 0$ the bifurcation diagram will resemble figure 5(*c*), which is just the inverse of figure 5(*b*). Here the first transition is to down hexagons

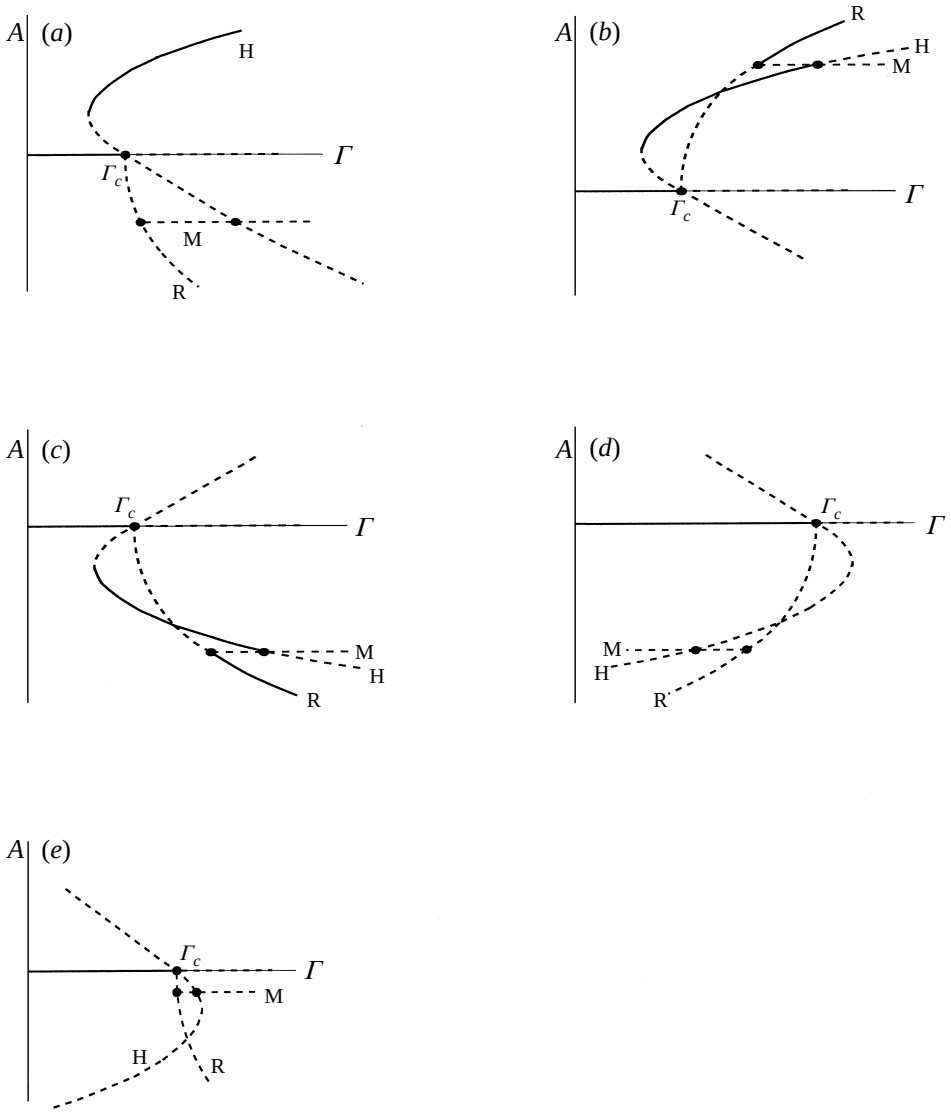

FIGURE 5. Bifurcation diagrams according to third-order nonlinear theory for rolls (R), hexagons (H) and mixed mode solutions (M). 'Up' hexagons have $A > 0$ and 'down' hexagons have $A < 0$. Stable solutions are represented by solid lines and unstable solutions by dashed lines. (*a*) $\tilde{\chi}_2 < 0$, $\tilde{\chi}_3 < 0$, $\tilde{\chi}_6 > \tilde{\chi}_5 > 0$; (*b*) $\tilde{\chi}_2 < 0$, $\tilde{\chi}_3 < 0$, $\tilde{\chi}_5 > \tilde{\chi}_6 > 0$; (*c*) $\tilde{\chi}_2 > 0$, $\tilde{\chi}_3 < 0$, $\tilde{\chi}_5 > \tilde{\chi}_6 > 0$; (*d*) $\tilde{\chi}_2 < 0$, $\tilde{\chi}_3 < 0$, $\tilde{\chi}_5 < \tilde{\chi}_6 < 0$; (*e*) $\tilde{\chi}_2 < 0$, $\tilde{\chi}_3 < 0$, $2\tilde{\chi}_5 < -\tilde{\chi}_6 < \tilde{\chi}_5 < 0$.

which lose stability to rolls at higher values of Γ. In all three of the above cases the first observed pattern would be hexagons (either up or down).

If $\tilde{\chi}_2 < 0$, $\tilde{\chi}_3 < 0$ and $\tilde{\chi}_5 < \tilde{\chi}_6 < 0$ the bifurcation diagram will resemble figure 5(*d*) and if $\tilde{\chi}_2 < 0$, $\tilde{\chi}_3 < 0$ and $2\tilde{\chi}_5 < -\tilde{\chi}_6 < \tilde{\chi}_5 < 0$ it will resemble figure 5(*e*). In these two cases both the hexagon branches and the rolls are unstable and physically we might expect a transition to another steady-state pattern (requiring an analysis on a more general lattice) or to an unsteady pattern. We have carried out the analysis on a square lattice and we find that, as usual, the bifurcation to squares is a pitchfork.

The stability of the branches of this bifurcation and whether it is sub- or supercritical depend on the values of four parameters, χ_1, χ_3 and two more.

Amplitude equations like (4.8) are generic for this type of problem and have been widely studied. The bifurcation diagrams in figure 5 are similar to those of Buzano & Golubitsky (1983) and Golubitsky *et al.* (1984). They indicate that, when either hexagons or rolls are stable near the onset of bioconvection, hexagons will be preferred. Whether these hexagons have flow up or down in the centre and whether or not they are stable depends on the values of the χ_i which must be found numerically.

5. Numerical results for $k_c \neq 0$

The form of the bifurcation diagram depends on the values of the χ_i in equation (4.8) which we find by solving the $O(\epsilon)$ and $O(\epsilon^2)$ equations numerically and then evaluating the integrals listed in the Appendix. The values of k_c, Γ_c and the χ_i depend on β and γ only via the combination $\beta\gamma$. Therefore we only have three parameters to consider: $\beta\gamma$, δ and Sc. However, we must still ensure that the values of β and γ chosen are such that the chamber is shallow (equation (3.3)). The $O(\epsilon)$ equations form an eigenvalue problem with Γ_c as the eigenvalue. In order to solve the system an extra, arbitrary boundary condition, which simply scales the solutions, must be imposed. We impose $N(z) = 1$ at $z = 0$. The system is solved using a routine kindly provided by Dr D. R. Moore (Cash & Moore 1980). The adjoint problem for $\boldsymbol{V}$, which is also an eigenvalue problem, is solved using the same routine by imposing the extra boundary condition $V_2 = 1$ at $z = 0$. The eigenvalue Γ_c is the same in both cases. Having found the first-order functions we can calculate χ_1, χ_2 and χ_3 by numerical integration.

The second-order functions are found by numerical solution of four sets of coupled ordinary differential equations using a finite difference technique and Newton iterations. The solvability condition appears in one of these four sets which requires the computed value of χ_2/χ_3. Having found the first- and second-order functions, we can find χ_5 and χ_6 by numerical integration. The values of k_c, Γ_c, χ_1, χ_2, χ_3, χ_5 and χ_6 for various values of $\beta\gamma$, δ and Sc are given in table 1.

When $\beta\gamma \gg 1$ a significant cell boundary layer forms at the free surface (see figure 2) which results in a very steep gradient in n_0 close to the free surface. This makes the numerical solution slightly more difficult and we need to use a grid with points clustered near the free surface.

The first-order equations do not contain Sc, hence the values of k_c, Γ_c and χ_3 depend only on δ and $\beta\gamma$ and are independent of Sc. The values of the other χ_i are more or less independent of Sc when $Sc \geqslant O(1)$, for given $\beta\gamma$ and δ (see $Sc = 2$ and $Sc = 7700$ in table 1), but they are significantly affected for $Sc \ll 1$ ($Sc = 0.01$ in table 1). In all cases studied, down hexagons are predicted for $Sc = 0.01$, even where that is not the case at higher Sc. However 0.01 is an unrealistically small value for the Schmidt number (see below) and we now concentrate our attention on the effect of $\beta\gamma$ and δ at more realistic values of Sc (2 and 7700).

For $\delta = 1$ we computed values of the χ_i for $\beta\gamma$ =0.05, 1 and 50. For $\beta\gamma = 0.05$, $\tilde{\chi}_2 > 0$, $\tilde{\chi}_3 < 0$ and $\tilde{\chi}_5 > \tilde{\chi}_6 > 0$, indicating that the first stable transition from the steady state is to down hexagons (see figure 5*c*). For $\beta\gamma = 1$, $\tilde{\chi}_2$ becomes negative, $\tilde{\chi}_6 - \tilde{\chi}_5$ becomes positive and the first stable transition is to up hexagons (figure 5*a*). At large $\beta\gamma$ (= 50), $\tilde{\chi}_6 - \tilde{\chi}_5$ becomes negative again but the first stable transition is still to up hexagons (figure 5*b*).

For $\delta = 3$ and $\beta\gamma = 1$, $\tilde{\chi}_2 < 0$, $\tilde{\chi}_3 < 0$ and $2\tilde{\chi}_5 < -\tilde{\chi}_6 < \tilde{\chi}_5 < 0$. In this case both hexagon branches are subcritical and unstable and the rolls are supercritical and unstable (see figure 5*e*). When the value of δ is increased to 7, 10 or 16, $\tilde{\chi}_2 < 0$, $\tilde{\chi}_3 < 0$ and $\tilde{\chi}_5 < \tilde{\chi}_6 < 0$. In this case both the roll and hexagon branches are subcritical and unstable (figure 5*d*).

Note that $|\ \tilde{\chi}_2\ |$ is small (though not always very small) compared to $2\tilde{\chi}_5 + \tilde{\chi}_6$ for all parameter values listed except $\beta\gamma = 50$, $\delta = 1$ and $Sc = 7700$. Therefore the mixing of second- and third-order terms in the analysis in the previous section was reasonably justified except in this one case. Since χ_2 is small when the problem is almost symmetric (Golubitsky *et al.* 1984), it is not surprising that it becomes large for large $\beta\gamma$ when the basic density distribution is very asymmetric with a high concentration of cells near the upper surface.

Experimental observations (figure 1) indicate that the first bifurcation from the steady state is to down hexagons. This bifurcation occurs when the suspension is approximately 0.5 mm deep. Hillesdon *et al.* (1995) gave estimates of the values of the parameters applicable to the experiment of Kessler *et al.* (1994) as

$$\beta = 7h^2, \quad \gamma = 15h, \quad \delta = 7, \quad Sc = 7700, \tag{5.1}$$

where h is the depth of the chamber in mm. Hillesdon & Pedley (1996) suggested $\delta = 16$ as a realistic value instead, the difference being due to taking $D_C = 2.12 \times 10^3$ rather than $D_C = 10^3$.

The results in table 1 indicate that for realistically large values of Sc and $\delta = 3, 7$ and 16 both up and down hexagons and rolls are unstable, whereas for $\delta = 1$ the model predicts that the first transition from the steady state will be to stable hexagons. This suggests that previous estimates of δ were too large. A smaller value of δ corresponds to a larger value of D_{N0} which corresponds to a greater contribution from random aspects of cell swimming.

Using an analogy with kinetic theory, Hillesdon *et al.* (1995) estimated D_{N0} as $\frac{1}{3}V_s^2\tau$ where V_s is the average cell swimming velocity and τ is the cell velocity correlation time. They used $V_s = 20\ \mu\text{m s}^{-1}$ and $\tau = 1$ s, values which are similar to those quoted for *Escherichia coli*, another flagellated bacterium (Berg 1983); larger values of V_s or τ for *B. subtilis* would give the required larger value for D_{N0}. The preliminary data on *B. subtilis* trajectories measured by Kessler *et al.* (1995) do indeed indicate longer sequences of straight trajectory than for *E. coli* and therefore a smaller value of δ is appropriate. More detailed measurements should however be made on the trajectories of *B. subtilis* and analysis performed similar to that of Hill & Häder (1997) for the alga *C. nivalis*.

The numerical results in table 1 also indicate that the model only predicts the formation of stable down hexagons (as seen experimentally) for realistic Sc if the value of $\beta\gamma$ is small (e.g. 0.05). For larger values of $\beta\gamma$ up hexagons are predicted. Biologically, a small value of $\beta\gamma$ corresponds to a small value of K_0 (low oxygen consumption by the bacteria), a small value of N_0 (low initial concentration of bacteria), a large value of $C_0 - C_{min}$ or a large value of D_{N0} (large contribution from random cell swimming). This last is most likely to be relevant, as discussed above.

For the parameter values which predict down hexagons ($\beta\gamma = 0.05$, $\delta = 1$) the model predicts a critical wavenumber of 1.371 (table 1) which corresponds to hexagons of wavelength approximately 2.9 mm. This compares reasonably well with the observed wavelength of the hexagons (figure 1) which is approximately 1.7 mm.

6. Weakly nonlinear analysis: $k_c = 0$

A slightly different analysis is needed for regions of parameter space in which the critical wavenumber k_c is zero. For simplicity we consider here the two-dimensional case only; in the three-dimensional case equation (6.7) is replaced by a partial differential equation in two spatial variables, the solution of which is beyond the scope of this paper. The method is similar to that used by Chapman & Proctor (1980) and Depassier & Spiegel (1981). We aim to derive an equation for the horizontal planform function f and then seek solutions which are periodic in a box of length L.

For disturbances close to critical the horizontal variation will be much more gradual than the vertical variation so that we can rescale the horizontal variable x as $X = \epsilon x$, z remaining the same. In the two-dimensional case we can describe the fluid velocity using a streamfunction: $\boldsymbol{u} = -\nabla \times \boldsymbol{\psi}\hat{\boldsymbol{y}}$. The pressure p can be eliminated from the governing equations by taking the curl of equation (2.7):

$$\nabla \times \left[Sc^{-1} \left(\frac{\partial \boldsymbol{u}}{\partial t} + (\boldsymbol{u} \cdot \nabla)\boldsymbol{u} \right) \right] = \nabla^4 \psi - \Gamma \frac{\partial n}{\partial x}. \tag{6.1}$$

We define ϵ by

$$\Gamma = \Gamma_c + \epsilon^2 \Gamma_1 ,$$

expand the variables as

$$\begin{aligned} n &= n_0 + \epsilon^2 n_1 + \epsilon^4 n_2 + \epsilon^6 n_3 + \ldots , \\ \theta &= \theta_0 + \epsilon^2 \theta_1 + \epsilon^4 \theta_2 + \epsilon^6 \theta_3 + \ldots , \\ \psi &= \epsilon^3 \psi_1 + \epsilon^5 \psi_2 + \ldots , \end{aligned}$$

and consider a slow timescale $\tau = \epsilon^4 t$. The expanded variables are substituted into equations (2.5), (2.6) and (6.1) and powers of ϵ equated.

$O(1)$ in equations (2.5) and (2.6) gives the analytic solution for the steady state $n_0(z)$ and $\theta_0(z)$ as before. $O(\epsilon^2)$ in equations (2.5) and (2.6) and $O(\epsilon^3)$ in equation (6.1) give homogeneous equations for n_1, θ_1 and ψ_1 which can be solved, subject to the boundary conditions, without the need for a solvability condition. The solution takes the form

$$n_1 = N(z)\, f(X,\tau), \quad \theta_1 = C(z)\, f(X,\tau), \quad \psi_1 = \Gamma_c\, \Psi(z)\, \frac{\partial}{\partial X} f(X,\tau), \tag{6.2a–c}$$

where the functions N, C and Ψ have to be calculated numerically, except in the limit $\beta\gamma \ll 1$, because the coefficients of the equations involve $n_0(z)$ and $\theta_0(z)$ from equations (3.1) and (3.2).

In order to satisfy the condition on conservation of cells (equation (2.9)) we require that

$$\int\int n_1 \, \mathrm{d}z \, \mathrm{d}X = 0 . \tag{6.3}$$

This means that either $\int_0^1 N \, \mathrm{d}z = 0$ or $\int f(X,\tau) \, \mathrm{d}X = 0$ over some suitable range of X. Since it is not possible to enforce $\int_0^1 N \, \mathrm{d}z = 0$, we will enforce the condition on f. We will be looking for solutions which are periodic in a box of length L so we impose $\int_0^L f(X,\tau) \, \mathrm{d}X = 0$. There is an arbitrariness in the choice of the scaling of f in (6.2); we choose the scaling such that $\int_0^L f^2 \, \mathrm{d}X = 1$.

$O(\epsilon^4)$ in equation (2.5) and (2.6) and $O(\epsilon^5)$ in equation (6.1) give three inhomogeneous equations for n_2, θ_2 and ψ_2. The boundary conditions on these equations can

$\beta\gamma$	δ	Sc	k_c	Γ_c	χ_1	χ_2	χ_3	χ_5	χ_6	
0.05	1.0	0.01	1.371	10241.81	12.18	123.89	-2.27×10^{-4}	1385250	632142	down hexagons
0.05	1.0	2	1.371	10241.81	1.343	4.980	-2.27×10^{-4}	5920.17	5435.74	down hexagons
0.05	1.0	7700	1.371	10241.81	1.288	4.383	-2.27×10^{-4}	5931.95	5429.54	down hexagons
1.0	1.0	0.01	1.58	624.686	11.80	4.628	-3.77×10^{-3}	8026.86	1448.51	down hexagons
1.0	1.0	2.0	1.58	624.686	0.890	−0.906	-3.77×10^{-3}	8.351	8.608	up hexagons
1.0	1.0	100	1.58	624.686	0.836	−0.933	-3.77×10^{-3}	8.073	8.458	up hexagons
1.0	1.0	7700	1.58	624.686	0.835	−0.934	-3.77×10^{-3}	8.069	8.456	up hexagons
50.0	1.0	7700	1.937	327.585	1.78×10^{-2}	-7.45×10^{-4}	-5.68×10^{-4}	1.19×10^{-4}	3.61×10^{-5}	up hexagons
1.0	3.0	0.01	1.085	734.474	4.920	0.641	-1.22×10^{-3}	1476.54	521.00	down hexagons
1.0	3.0	7700	1.085	734.474	0.621	−0.413	-1.22×10^{-3}	−0.766	0.986	hexagons unstable
1.0	7.0	7700	0.769	757.972	0.592	−0.214	-5.74×10^{-4}	−3.510	−0.486	hexagons unstable
1.0	10.0	2	0.663	761.538	0.593	−0.160	-4.23×10^{-4}	−4.577	−0.829	hexagons unstable
1.0	10.0	7700	0.663	761.538	0.587	−0.160	-4.23×10^{-4}	−4.715	−0.903	hexagons unstable
1.0	16.0	7700	0.547	763.896	0.584	−0.110	-2.87×10^{-4}	−7	−1.4	hexagons unstable

TABLE 1. Numerical results for the hexagonal lattice in the case $k_c \neq 0$.

		Numerical						Analytic					
$\beta\gamma$	δ	ζ_1	ζ_2	ζ_3	ζ_4	ζ_5	Γ_c	ζ_1	ζ_2	ζ_3	ζ_4	ζ_5	Γ_c
0.01	10	0.997	1.724×10^{-5}	0.993	0.0487	1.977	57803.87	0.997	1.724×10^{-5}	0.993	0.050	2	57804.069
0.01	16	0.997	1.724×10^{-5}	0.993	0.0595	1.977	57803.87	0.997	1.724×10^{-5}	0.993	0.061	2	57804.069
0.05	10	0.984	8.390×10^{-5}	0.968	0.0431	1.887	11723.11	0.984	8.382×10^{-5}	0.951	0.050	2	11724.069
0.05	16	0.984	8.390×10^{-5}	0.968	0.0538	1.887	11723.11	0.984	8.382×10^{-5}	0.951	0.061	2	11724.069
0.5	16	0.853	6.331×10^{-4}	0.741	0.0101	1.176	1347.789	0.856	5.696×10^{-4}	0.761	0.061	2	1356.069
0.5	30	0.853	6.331×10^{-4}	0.741	0.0169	1.176	1347.789	0.856	5.696×10^{-4}	0.761	0.069	2	1356.069

TABLE 2. Numerical results in the case $k_c = 0$.

be satisfied only if the solvability condition

$$\int_0^1 \left(\frac{\partial^2 n_1}{\partial X^2} + \frac{\mathrm{d}n_0}{\mathrm{d}z}\frac{\partial \psi_1}{\partial X} - \gamma n_0 \frac{\partial^2 \theta_1}{\partial X^2} \right) \mathrm{d}z = 0 \tag{6.4}$$

holds. Substituting n_1, θ_1 and ψ_1 into (6.4) implies that

$$\Gamma_c = \frac{\zeta_1}{\zeta_2} \tag{6.5}$$

where ζ_1 and ζ_2 are given in the Appendix.

To solve the equations for n_2, θ_2 and ψ_2 we pose a solution

$$n_2 = J_1(z) f_{XX} + J_2(z) f^2,$$
$$\theta_2 = G_1(z) f_{XX} + G_2(z) f^2,$$
$$\psi_2 = \Gamma_c D(z) f_{XXX} + \Gamma_c E(z) f f_X + \Gamma_1 F(z) f_X,$$

which results in ordinary differential equations for J_1, J_2, G_1, G_2, D, E and F which can be solved numerically, or analytically if $\beta\gamma \ll 1$. F satisfies the same differential equation and boundary conditions as Ψ; hence $F \equiv \Psi$.

Note that in order to satisfy the integral condition $\iint n_2 \,\mathrm{d}z = 0$, we require either $\int_0^1 J_1 \mathrm{d}z = 0$ or $\int_0^L f_{XX}\ \mathrm{d}X = 0$ and $\int_0^1 J_2\ \mathrm{d}z = 0$. Later we impose the periodic boundary conditions $f_X = 0$ at $X = 0, L$, hence we only require $\int_0^1 J_2\ \mathrm{d}z = 0$.

The solvability condition at the next order in ϵ gives the equation

$$\zeta_3 f_\tau + \zeta_4 f_{XXXX} + \zeta_5 \left(f_X^2 + f f_{XX} \right) - \Gamma_1 \zeta_2 f_{XX} = 0, \tag{6.6}$$

where the ζ_i are given in the Appendix. The same equation, although with opposite signs for the coefficients ζ_2 and ζ_5, was found by Depassier & Spiegel (1981) for compressible convection in a layer of perfect gas with fixed heat flux on the boundaries.

Since we are looking for solutions to (6.6) which are periodic in a box of length L we impose the boundary conditions $f_X = f_{XXX} = 0$ at $X = 0$, L; these conditions mean zero streamfunction, shear stress, cell gradient and oxygen gradient across the ends of the box. We can then rescale the variables to eliminate L. We let

$$\eta = \frac{X}{L}, \quad T = \frac{\zeta_4}{L^4 \zeta_3}\tau, \quad \mathscr{F} = \frac{\zeta_5 L^2}{\zeta_4} f,$$

so that equation (6.6) becomes

$$\mathscr{F}_T + \mathscr{F}_{\eta\eta\eta\eta} + \mathscr{F}_\eta^2 + \mathscr{F}\mathscr{F}_{\eta\eta} - \Gamma_1 L^2 \frac{\zeta_2}{\zeta_4} \mathscr{F}_{\eta\eta} = 0, \tag{6.7}$$

subject to boundary conditions:
at $\eta = 0$

$$\mathscr{F}_{\eta\eta\eta} = \mathscr{F}_\eta = 0\,;$$

at $\eta = 1$

$$\mathscr{F}_{\eta\eta\eta} = \mathscr{F}_\eta = 0.$$

We also have the integral condition

$$\int_0^1 \mathscr{F}\ \mathrm{d}\eta = 0 \tag{6.8}$$

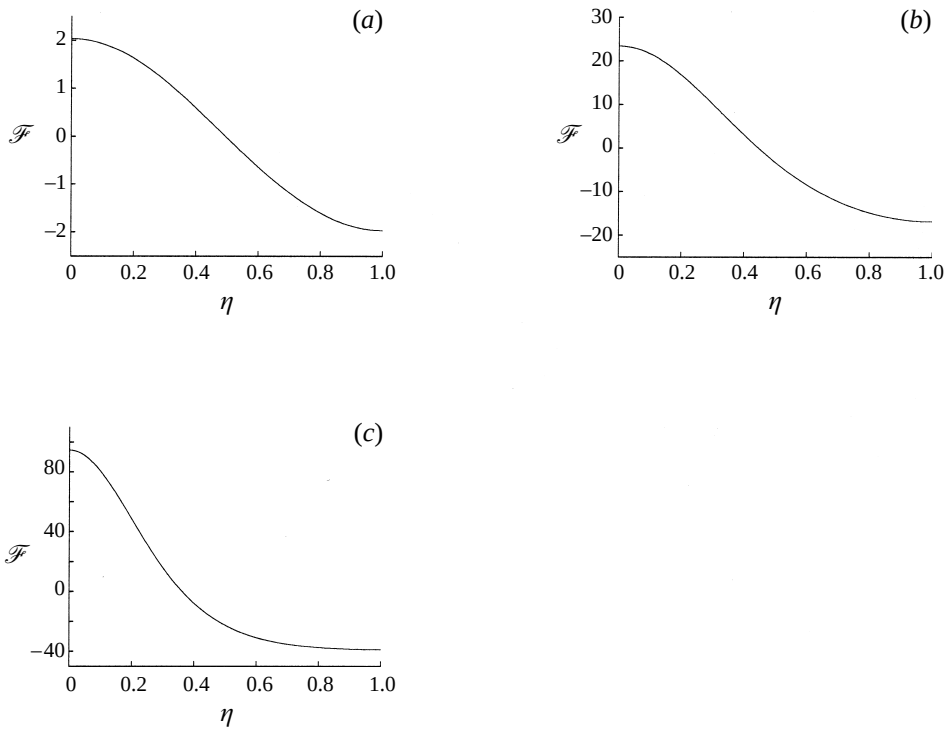

FIGURE 6. The solution $\mathscr{F}$ in the case $k_c = 0$. (*a*) $P = 1$; (*b*) $P = 100$; (*c*) $P = 1000$.

and the scaling condition

$$\int_0^1 \mathscr{F}^2 \, \mathrm{d}\eta = \frac{\zeta_5^2}{\zeta_4^2} L^3 \, .$$

We now consider stationary solutions with $\mathscr{F}_T = 0$ and integrate (6.7) twice with respect to η to obtain

$$\mathscr{F}_{\eta\eta} + \tfrac{1}{2}\mathscr{F}^2 - \Gamma_1 L^2 \frac{\zeta_2}{\zeta_4} \mathscr{F} = P \, , \tag{6.9}$$

where

$$P = \frac{\zeta_5^2}{2\zeta_4^2} L^3 = \frac{1}{2} \int_0^1 \mathscr{F}^2 \, \mathrm{d}\eta \, .$$

Equation (6.9), the boundary conditions on $\mathscr{F}_\eta$ and (6.8) constitute an eigenvalue problem with $\Gamma_1 L^2 \zeta_2/\zeta_4$ as the eigenvalue. We can solve equation (6.9) numerically for a given value of P; solutions $\mathscr{F}$ of this equation for different values of P are shown in figure 6. The value of the eigenvalue $\Gamma_1 L^2 \zeta_2/\zeta_4$ changes with the value of P (see figure 7). For small values of P (i.e. small values of L) $\Gamma_1 L^2 \zeta_2/\zeta_4$ is positive. As P increases (i.e. L increases), $\Gamma_1 L^2 \zeta_2/\zeta_4$ decreases and for $P > P_{crit}$ it becomes negative, i.e. $\Gamma_1 \zeta_2/\zeta_4$ is negative for $L > \left(2P_{crit}\zeta_4^2/\zeta_5^2\right)^{1/3}$.

The behaviour of the system depends on the values of the ζ_i in equations (6.5) and (6.6). In order to calculate these quantities we need to solve the first- and second-order equations and integrate to find the ζ_i. In general this must be done numerically but for $\beta\gamma \ll 1$ an analytic solution exists. In § 6.1 we present this analytic solution and in § 6.2 we present the numerical solution for a range of parameter values and compare

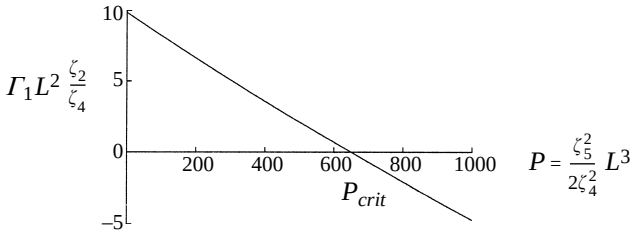

FIGURE 7. Graph showing the variation of $\Gamma_1 L^2 \zeta_2/\zeta_4$ with $P = (\zeta_5^2/2\zeta_4^2)L^3$ in the case where $k_c = 0$.

it to the analytic solution. As in the $k_c \neq 0$ case, β and γ affect the result only via the combination $\beta\gamma$; the individual values of β and γ are not important provided that they are such that the chamber is shallow.

6.1. *Calculation of the ζ_i: analytic solution for $\beta\gamma \ll 1$*

In the limit $\beta\gamma \ll 1$, Hillesdon & Pedley (1996) give the steady-state solutions as

$$n_0 = 1 + \tfrac{1}{2}\left(z^2 - 2z + \tfrac{2}{3}\right)\beta\gamma + \tfrac{1}{6}\left(z^4 - 4z^3 + 5z^2 - 2z + \tfrac{7}{24}\right)\beta^2\gamma^2 + O\left(\beta^3\gamma^3\right),$$

$$\frac{\mathrm{d}\theta_0}{\mathrm{d}z} = \beta(z-1) - \tfrac{1}{6}\beta^2\gamma\,(1-z)\left(z^2 - 2z\right) + O\left(\beta^3\gamma^2\right).$$

Hillesdon & Pedley also carried out the linear stability analysis in the $\beta\gamma \ll 1$ limit and found that an analytic solution was possible for small wavenumbers ($k^2 = O(\beta\gamma)$) giving $\Gamma_c = 576/\beta\gamma + O(1)$. This suggests that an analytic solution for the weakly nonlinear problem in the $k_c = 0$ case is possible in the limit $\beta\gamma \ll 1$.

The first-order equations have a solution of the form

$$N = \sum_{i=0}^{\infty} N_i(z)\,(\beta\gamma)^i, \quad C = \sum_{i=0}^{\infty} C_i(z)\,\beta(\beta\gamma)^i, \quad \Psi = \sum_{i=0}^{\infty} \Psi_i(z)\,(\beta\gamma)^i,$$

where N_i, C_i, and Ψ_i are polynomials in z. Having found these functions we can use (A 6), (A 7) and (A 8) to find ζ_1, ζ_2 and ζ_3:

$$\zeta_1 = 1 - \frac{\beta\gamma}{3} + \frac{4}{45}\beta^2\gamma^2 + O(\beta^3\gamma^3),$$
$$\zeta_2 = \frac{\beta\gamma}{576} - \frac{361}{302400}\beta^2\gamma^2 + O(\beta^3\gamma^3),$$
$$\zeta_3 = 1 - \beta\gamma + \frac{17}{45}\beta^2\gamma^2 + O(\beta^3\gamma^3).$$

We can then use (6.5) to find

$$\Gamma_c = \frac{576}{\beta\gamma} + \frac{35712}{175} + O(\beta\gamma). \tag{6.10}$$

The second-order functions can be found as expansions in powers of $\beta\gamma$ in the same way as the first-order functions and used to find ζ_4 and ζ_5 from equations (A 9) and (A 10):

$$\zeta_4 = \frac{11881}{150150} - \frac{6229}{21450\delta} + O(\beta\gamma), \tag{6.11}$$

$$\zeta_5 = 2 + O(\beta\gamma); \tag{6.12}$$

ζ_4 is positive for $\delta \gtrsim 3.67$ and this is always true when $k_c = 0$ (see figure 4). Hence $\zeta_1 \ldots \zeta_5$ are always positive for small $\beta\gamma$.

6.2. *Calculation of the ζ_i: numerical solution*

The first-order equations are solved using a finite difference technique and Newton iterations. It is necessary to impose an extra boundary condition, which simply scales the solutions. We impose $N = 1$ at $z = 0$. ζ_1, ζ_2 and ζ_3 are then found by numerical integration and the value of Γ_c is calculated from (6.5). The second-order equations are solved using the same routine as in § 5 and ζ_4 and ζ_5 are calculated by numerical integration. The numerically calculated values of the ζ_i and Γ_c for various values of $\beta\gamma$ and δ are shown in table 2, where we have included the relevant values of the ζ_i and Γ_c according to the analytic solution for comparison.

Only a small region of parameter space is both realistic and relevant for the $k_c = 0$ case, because in general δ must be unrealistically large (see figure 4); the constants $\zeta_1 \ldots \zeta_5$ are all positive for all the parameter values which we have considered.

6.3. *Discussion of results*

The variation of Γ_1 with L shown in figure 7 may be thought of in two ways. We can consider the problem as defined over an infinite horizontal domain on which the system is left to find its own lengthscale. In this case the value of the lengthscale L will depend on the value of the Rayleigh number Γ. For $\zeta_2/\zeta_4 > 0$, as Γ increases the first instabilty will be subcritical ($\Gamma_1 < 0$) and the wavelength L of the patterns formed will be very large. If $\zeta_2/\zeta_4 < 0$, then as Γ increases the first instabilty will again be subcritical and will occur at $\Gamma_1 L^2 \zeta_2/\zeta_4 \approx 9.9$. In this case we would expect the wavelength L of the patterns formed to be very small. If L is very small the original assumption that the wavelength of the patterns is large compared to the depth of the layer will no longer hold; however, since we have found that the coefficients ζ_i are always positive we need consider the $\zeta_2/\zeta_4 < 0$ case no further.

Alternatively we can consider the problem as being confined to a box of horizontal extent H. In this case the first instabilities must have $L < H$. For $\zeta_2/\zeta_4 > 0$ this constraint imposes a minimum value on Γ_1 which may be positive or negative depending on whether $(\zeta_5^2/2\zeta_4^2)H^3$ is less than or greater than P_{crit}. If $(\zeta_5^2/2\zeta_4^2)H^3 < P_{crit}$ the minimum value of Γ_1 is positive. Hence as Γ increases the first bifurcation will be supercritical and the resulting weak patterns will have wavelength H. If $(\zeta_5^2/2\zeta_4^2)H^3 > P_{crit}$ the minimum value of Γ_1 is negative. In this case, as Γ increases the first bifurcation will be subcritical and will be to finite-amplitude patterns of wavelength H.

7. Conclusion

In this paper we have carried out a weakly nonlinear analysis to predict the patterns formed at the onset of bioconvection in a suspension of the oxytactic bacterium *Bacillus subtilis*. We use the model described in Hillesdon & Pedley (1996).

The linear stability of the steady state depends on whether the Rayleigh number Γ is greater or less than the neutral value $\Gamma_n(k)$ where k is the wavenumber of the disturbance. The most unstable wavenumber, k_c, can be either zero or non-zero, depending on the values of the parameters $\beta\gamma$ and δ. We have carried out a weakly nonlinear analysis to investigate the patterns formed at the onset of convection in both of these cases.

For the $k_c \neq 0$ case we considered patterns on a hexagonal lattice and predicted that the first transition from the steady state will be to hexagons, as long as the diffusivity ratio δ is not too large. Whether these hexagons are stable and whether they are up or down hexagons depends on the values of the parameters $\beta\gamma$ and δ. We obtained numerical results for the hexagonal lattice which enabled us to draw bifurcation diagrams for different regions of parameter space. For values of δ larger than about 3 both hexagons and rolls are subcritical and unstable. For values of δ smaller than this hexagons are stable (to disturbances that are consistent with the hexagonal lattice at least). For small $\beta\gamma$ the first bifurcation is to down hexagons and for larger $\beta\gamma$ the first bifurcation is to up hexagons.

Experiments in a slightly tilted chamber show that the first bifurcation from the steady state is to down hexagons. The model predicts this bifurcation to down hexagons, but only for values of $\beta\gamma$ and δ which are smaller than previous estimates of these parameters. A smaller value of δ would result from a larger value of the cell diffusivity D_{N0}. A larger value of D_{N0} would also result in the required smaller value of $\beta\gamma$, but a smaller value of $\beta\gamma$ could also come from a smaller value of the oxygen consumption K_0 or of the chemotaxis coefficient a. More detailed measurements of these quantities would clearly be desirable.

For the case where the critical wavenumber k_c is zero we carried out a two-dimensional analysis. We derived an equation (6.6) describing the evolution of the horizontal planform f and looked for steady solutions to this which are periodic in a box of length L. The wavelength, L, of the patterns formed and whether they are sub- or supercritical depends on Γ_1, the deviation of Γ from its critical value Γ_c.

We carried out both a numerical solution and an analytic solution for the region $\beta\gamma \ll 1$. We found that for $\Gamma_1 < 0$, i.e. Γ subcritical, the wavelength of the patterns is large and as Γ_1 increases the wavelength of the patterns decreases. However, we have not investigated the stability of these solutions or the possibility that subcritical solutions may turn over at higher order (as in the $k_c \neq 0$ case).

Throughout this paper we have considered only the shallow chamber case in which all the bacteria have sufficient oxygen to be active. The results may be different in the deep chamber. As suggested previously, the model we have used may be inadequate in other ways. The orientation of cells by fluid shear (gyrotaxis) has proved to be important in algal bioconvection and the cell conservation equation should presumably contain a term to describe it. It may also be useful to consider a more detailed model for chemotaxis, which takes account of the details of the chemotaxis mechanism (cf. Armitage, Havelka & Sockett 1990). A self-consistent model has been developed for gyrotactic algae which includes both deterministic and random aspects of cell swimming in a probability density function for the cell swimming direction (Pedley & Kessler 1990); more detailed experimental information about the behaviour of individual cells (cf. Kessler *et al.* 1995) may help us to develop such a model for chemotactic bacteria.

The authors would like to thank the Engineering and Physical Sciences Research Council for their financial support, A.M.M. for a Research Studentship and T.J.P. for a Senior Fellowship. We would also like to thank Professor J. O. Kessler for originating this research and for the use of his photograph of the experiments; Dr N. A. Hill, Dr R. B. Hoyle, Dr P. C. Matthews, Dr M. R. E. Proctor and Dr A. Skeldon for many helpful discussions; and Dr D. R. Moore for use of the ordinary differential equation solver NRK.

Appendix

This Appendix contains the expressions for the χ_i and the ζ_i which appear in the solvability conditions and evolution equations. The functions J_i, G_i and E_i in χ_5 and χ_6 are the solutions to the second-order differential equations.

$$\chi_1 = \int_0^1 Sc^{-1}V_1(W'' - k^2W) + V_2N + \frac{1}{\delta}V_3C \, \mathrm{d}z, \tag{A 1}$$

$$\begin{aligned}\chi_2 = \int_0^1 \Big[& V_1Sc^{-1}(W'W'' + \tfrac{1}{2}WW''' - \tfrac{3}{2}k^2WW') \\ & + V_2(WN' + \tfrac{1}{2}W'N - \tfrac{1}{2}\gamma k^2CN + \gamma N'C' + \gamma NC'') \\ & + \frac{V_3}{\delta}(WC' + \tfrac{1}{2}W'C)\Big] \mathrm{d}z + \left(V_2\gamma NC'\right)\big|_{z=0},\end{aligned} \tag{A 2}$$

$$\chi_3 = \int_0^1 V_1k^2N \, \mathrm{d}z, \tag{A 3}$$

$$\begin{aligned}\chi_5 = \int_0^1 \Big[& V_1Sc^{-1}k^2\left(-\tfrac{3}{4}k^2WE_6' - \tfrac{9}{4}k^2WE_7' - \tfrac{3}{4}k^2W'E_6 - \tfrac{15}{4}k^2W'E_7\right. \\ & \left. + \tfrac{1}{2}W'E_6'' + \tfrac{3}{2}W'E_7'' + \tfrac{1}{2}W''E_6' + \tfrac{1}{4}WE_6''' + \tfrac{3}{4}WE_7''' + \tfrac{1}{4}W'''E_6 - \tfrac{3}{4}W'''E_7\right) \\ & + V_2\left(\tfrac{1}{2}\gamma C'J_6' + \tfrac{1}{2}\gamma C''J_6 - \tfrac{1}{4}\gamma k^2CJ_6 + \tfrac{1}{2}\gamma C'J_7' + \tfrac{1}{2}\gamma C''J_7 + \tfrac{1}{4}\gamma k^2CJ_7\right. \\ & \left. + \gamma C'J_4' + \gamma C''J_4 - \gamma k^2CJ_4 - \tfrac{1}{4}\gamma k^2NG_6 - \tfrac{3}{4}\gamma k^2NG_7\right. \\ & \left. + \tfrac{1}{4}k^2NE_6' + \tfrac{3}{4}k^2NE_7' + \tfrac{1}{2}k^2N'E_6 + \tfrac{3}{2}k^2N'E_7 + WJ_4' + \tfrac{1}{2}WJ_6' + \tfrac{1}{2}WJ_7'\right. \\ & \left. + \tfrac{1}{4}W'J_6 + \tfrac{3}{4}W'J_7 + \gamma N'G_4' + \tfrac{1}{2}\gamma N'G_6' + \tfrac{1}{2}\gamma N'G_7' + \gamma NG_4'' + \tfrac{1}{2}\gamma NG_6'' + \tfrac{1}{2}\gamma NG_7''\right) \\ & + \frac{1}{\delta}V_3\left(\tfrac{1}{2}k^2C'E_6 + \tfrac{3}{2}k^2C'E_7 + \tfrac{1}{4}k^2CE_6' + \tfrac{3}{4}k^2CE_7'\right. \\ & \left. + WG_4' + \tfrac{1}{2}WG_6' + \tfrac{1}{2}WG_7' + \tfrac{1}{4}W'G_6 + \tfrac{3}{4}W'G_7\right)\Big] \mathrm{d}z \\ & + \left[V_2\gamma\left(C'J_4 + \tfrac{1}{2}C'J_6 + \tfrac{1}{2}C'J_7 + NG_4' + \tfrac{1}{2}NG_6' + \tfrac{1}{2}NG_7'\right)\right]\big|_{z=0},\end{aligned} \tag{A 4}$$

$$\begin{aligned}\chi_6 = \int_0^1 \Big[& V_1Sc^{-1}k^2\left(-3k^2WE_8' - 6k^2W'E_8 + 2W'E_8'' - W''E_8' + WE_8''' - 2W'''E_8\right) \\ & + V_2\left(\gamma J_4'C' + \gamma J_4C'' - \gamma k^2CJ_4 + \tfrac{1}{2}\gamma J_8'C' + \tfrac{1}{2}\gamma J_8C'' + \tfrac{1}{2}\gamma k^2CJ_8\right. \\ & \left. + \gamma N'G_4' + \gamma NG_4'' + \tfrac{1}{2}\gamma N'G_8' + \tfrac{1}{2}\gamma NG_8'' - \gamma k^2NG_8\right. \\ & \left. + WJ_4' + \tfrac{1}{2}WJ_8' + W'J_8 + k^2NE_8' + 2k^2N'E_8\right) \\ & + \frac{1}{\delta}V_3\left(2k^2C'E_8 + k^2CE_8' + WG_4' + \tfrac{1}{2}WG_8' + W'G_8\right)\Big] \mathrm{d}z \\ & + \left[\gamma V_2\left(C'J_4 + \tfrac{1}{2}C'J_8 + NG_4' + \tfrac{1}{2}NG_8'\right)\right]\big|_{z=0};\end{aligned} \tag{A 5}$$

$$\zeta_1 = \int_0^1 (N - \gamma n_0C) \, \mathrm{d}z, \tag{A 6}$$

$$\zeta_2 = \int_0^1 -\frac{\mathrm{d}n_0}{\mathrm{d}z}\Psi \, \mathrm{d}z, \tag{A 7}$$

$$\zeta_3 = \int_0^1 N \, \mathrm{d}z, \tag{A 8}$$

$$\zeta_4 = \int_0^1 \left(-J_1 - \Gamma_c D \frac{\mathrm{d}n_0}{\mathrm{d}z} + \gamma n_0 G_1 \right) \mathrm{d}z, \tag{A 9}$$

$$\zeta_5 = \int_0^1 \left(-2J_2 - \Gamma_c E \frac{\mathrm{d}n_0}{\mathrm{d}z} + 2\gamma n_0 G_2 + \gamma NC + \Gamma_c N \Psi' \right) \mathrm{d}z. \tag{A 10}$$

REFERENCES

Alt, W. 1994 Cell motion and orientation: theories of elementary behavior between environmental stimulation and autopoietic regulation. *Lecture Notes in Biomathematics Vol. 100, Frontiers in Mathematical Biology*. (ed. S. A. Levin). Springer.

Armitage, J. P., Havelka, W. A. & Sockett, R. E. 1990 Methylation-independent taxis in bacteria. In *Biology of the Chemotactic Response. 46th Symp. Soc. Gen. Microbiol.* pp. 177–197 (ed. J. P. Armitage & J. M. Lackie). Cambridge University Press.

Berg, H. C. 1983. *Random Walks in Biology*. Princeton University Press.

Berg, H. C. & Brown, D. A. 1972 Chemotaxis in *Escherichia coli* analysed by three-dimensional tracking. *Nature* **239**, 500–504.

Buzano, E. & Golubitsky, M. 1983 Bifurcation on the hexagonal lattice and the planar Bénard problem. *Phil. Trans. R. Soc. Lond.* A **308**, 617–667.

Cash, J. R. & Moore, D. R. 1980 A high order method for the numerical solution of two-point boundary value problems. *BIT* **20**, 44–52.

Chapman, C. J. & Proctor, M. R. E. 1980 Nonlinear Rayleigh–Bénard convection between poorly conducting boundaries. *J. Fluid Mech.* **101**, 759–782.

Depassier, M. C. & Spiegel, E. A. 1981 The large scale structure of compressible convection. *Astron. J.* **86**, 496–512.

Golubitsky, M., Swift, J. W. & Knobloch, E. 1984 Symmetries and pattern selection in Rayleigh-Bénard convection. *Physica* D **10**, 249–276.

Hill, N. A. & Häder, D. P. 1997 A biased random walk model for the trajectories of swimming micro-organisms. *J. Theor. Biol.* **186**, 503–526.

Hill, N. A., Pedley, T. J. & Kessler, J. O. 1989 Growth of bioconvection patterns in a suspension of gyrotactic micro-organisms in a layer of finite depth. *J. Fluid Mech.* **208**, 509–543.

Hillesdon, A. J. & Pedley, T. J. 1996 Bioconvection in suspensions of oxytactic bacteria: linear theory. *J. Fluid Mech.* **324**, 223–259.

Hillesdon, A. J., Pedley, T. J. & Kessler, J. O. 1995 The development of concentration gradients in a suspension of chemotactic bacteria. *Bull. Math. Biol.* **57**, 299–344.

Hoyle, R. B., McFadden, G. B. & Davis, S. H. 1996 Pattern selection with anisotropy during directional solidification. *Phil. Trans. R. Soc. Lond.* A **354**, 2915–2949.

Keller, E. F. & Segel, L. A. 1971*a* Model for chemotaxis. *J. Theor. Biol.* **30**, 225–234.

Keller, E. F. & Segel, L. A. 1971*b* Travelling bands of chemotactic bacteria. *J. Theor. Biol.* **30**, 235–249.

Kessler, J. O. 1985 Hydrodynamic focusing of motile algal cells. *Nature* **313**, 218–220.

Kessler, J. O., Hoelzer, M. A., Pedley, T. J. & Hill, N. A. 1994 Functional patterns of swimming bacteria. In *Mechanics and Physiology of Animal Swimming* (ed. L. Maddock, Q. Bone & J. M. V. Rayner). Cambridge University Press.

Kessler, J. O., Strittmatter, D. L., Swartz, D. L., Wiseley, D. A. & Wojciechowski, M. F. 1995 Paths and patterns: the biology and physics of swimming bacterial populations. In *Biological Fluid Dynamics* (*Symposia of the Society for Experimental Biology XLIX*), pp. 91–107 (ed. C. P. Ellington & T. J. Pedley). The Company of Biologists Limited.

Matthews, P. C. 1988 A model for the onset of penetrative convection. *J. Fluid Mech.* **188**, 571–583.

Pedley, T. J. & Kessler, J. O. 1990 A new continuum model for suspensions of gyrotactic micro-organisms. *J. Fluid Mech.* **212**, 155–182.

Pedley, T. J. & Kessler, J. O. 1992 Hydrodynamic phenomena in suspensions of swimming micro-organisms. *Ann. Rev. Fluid Mech.* **24**, 313–358.

Platt, J. R. 1961 'Bioconvection patterns' in cultures of free-swimming organisms. *Science* **133**, 1766–1767.

Wager, H. 1911 On the effect of gravity upon the movements and aggregation of *Euglena viridis, Ehrb* and other micro-organisms. *Phil. Trans. R. Soc. Lond.* B **201**, 333–390.